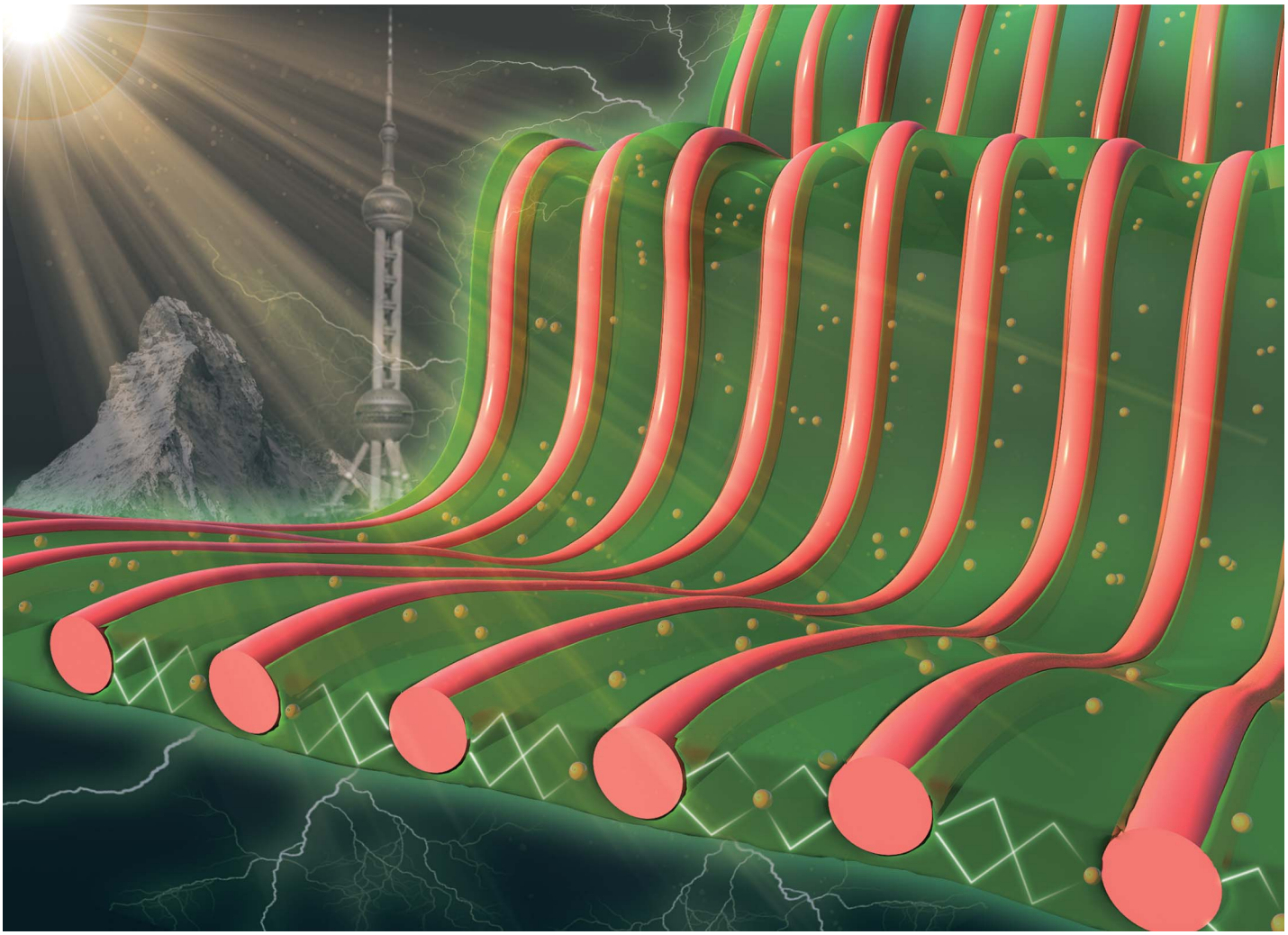

Highlighting research led by Prof. Xuemei Sun (Fudan University, China) and Dr Luciano F. Boesel (Empa, Switzerland).

Energy harvesting textiles: using wearable luminescent solar concentrators to improve the efficiency of fiber solar cells

For the first time, the integration of fiber solar cells (FSCs) and wearable luminescent solar concentrators (LSCs) has been demonstrated. The 84% enhancement in power conversion efficiency of FSCs is attributed to enlarged photon harvesting area and utilization of face-down surfaces of FSCs by attaching LSCs. The integrated device is flexible and powerful for wearable electronics.

As featured in:

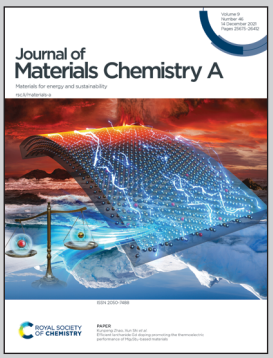

See Xuemei Sun, Luciano F. Boesel *et al.*, *J. Mater. Chem. A*, 2021, **9**, 25974.

ROYAL SOCIETY OF CHEMISTRY

rsc.li/materials-a

Registered charity number: 207890

Journal of Materials Chemistry A

PAPER

View Article Online
View Journal | View Issue

Cite this: J. Mater. Chem. A, 2021, 9, 25974

Energy harvesting textiles: using wearable luminescent solar concentrators to improve the efficiency of fiber solar cells†

Chieh-Szu Huang, ‡[bc] Xinyue Kang,‡[a] René M. Rossi, [b] Maksym V. Kovalenko, [cd] Xuemei Sun, *[a] Huisheng Peng [a] and Luciano F. Boesel *[b]

Received 12th June 2021
Accepted 23rd September 2021

DOI: 10.1039/d1ta04984d

rsc.li/materials-a

Fiber solar cells have attracted considerable interest in recent years for their agile integration with wearable electronics. They have the unique advantage of collecting light from all directions. However, in daily use, the incoming sunlight only covers the face-up surface area and a large portion of it is lost between fiber gaps, leading to an unexploited device efficiency. In this work, wearable luminescent solar concentrators (LSCs) are integrated with fiber solar cells to harvest additional photons and fully utilize the advantage of harvesting light from all directions. Wearable LSCs made from an amphiphilic polymer conetwork matrix and coumarin 6 luminescent dyes are applied to fiber dye-sensitized solar cells (FDSSCs). The results show a remarkable FDSSC power conversion efficiency enhancement of 84%, LSC concentration factor of 1.57, and device optical efficiency of 7.85%, attributed to LSC-assisted enlargement of the photon harvesting area, recycling of lost photons, and utilization of the complete surface of FDSSCs. Using a Monte Carlo ray-tracing simulation for optimizing the fibers' arrangement, a textile with multiple FDSSCs integrated with 3 cm^2 LSCs exhibits a high-power output of 0.89 mW. The device shows a sustainable power conversion efficiency even after 1000 bending cycles, which demonstrates its wearability. This is the first experimental and computational demonstration of the integration of FDSSCs and wearable LSCs as energy harvesting textiles, showcasing their potential as future wearable electronic systems.

Introduction

With the significant development of wearable electronic devices in recent years and the increased variety of functions per device, the rise in electricity consumption is inevitable.[1–3] For example, smart watches are promising portable devices endowed with multiple functions, such as communication, health monitoring, positioning, and navigation function. However, high electricity consumption and limited size of the device induced new challenges for the device operating life span. Photovoltaics (PVs) provide an optimal option for real-time power supply in a luminous environment as well as sustained power supply after being stored in batteries.[4] Nevertheless, the disadvantages of conventional PVs, *e.g.*, rigidity, bulkiness, and stacked-film structures, have restricted their integration with wearable devices and have hindered their niche applications in portable/wearable electronics. The quest for wearable PVs throws immense attention on the development of fiber solar cells.[5–8] Fiber solar cells provide an agile and robust integration with textiles and wearable electronics to adapt to the irregular shape and surface of the body parts with breathability and comfort, due to their fibrous structure, light weight, and flexibility.[9–11] Besides, the inherent fibrous structure can use incident photons from all directions equally, avoiding the pitfalls of angle-dependent efficiency. Nonetheless, the packed fiber solar cell array on textiles results in loss of photons in the gaps and a harvesting area employing only face-up surfaces, as shown in Fig. 1(a). Therefore, to achieve higher power conversion efficiency (PCE) per device, an optimal luminous environment to harvest penetrating photons

[a]State Key Laboratory of Molecular Engineering of Polymers, Department of Macromolecular Science and Laboratory of Advanced Materials, Fudan University, 2205 Songhu Road, Shanghai, 200438, China. E-mail: sunxm@fudan.edu.cn

[b]Empa, Swiss Federal Laboratories for Materials Science and Technology, Laboratory for Bio-mimetic Membranes and Textiles, Lerchenfeldstrasse 5, CH-9014 St. Gallen, Switzerland. E-mail: Luciano.Boesel@empa.ch

[c]ETH Zürich, Laboratory of Inorganic Chemistry, Department of Chemistry and Applied Bio-sciences, Vladimir-Prelog-Weg 1, CH-8093 Zürich, Switzerland

[d]Empa, Swiss Federal Laboratories for Materials Science and Technology Laboratory for Thin Films and Photovoltaics, Überlandstrasse 129, CH-8600 Dübendorf, Switzerland

† Electronic supplementary information (ESI) available. See DOI: 10.1039/d1ta04984d

‡ These authors contributed equally to this work.

and utilize the shadowed area of fiber solar cells *via* a wearable material is needed.

Luminescent solar concentrators (LSCs) are devices with transparent waveguide containing luminophores, absorbing direct and diffusive lights, activating luminophores, and concentrating the re-emitted light to the attached PVs.[12–15] Moreover, with the choice of luminophores for LSCs, the absorbed solar spectrum can be beneficially shifted according to the PVs' spectral responsive wavelength.[16,17] Adding LSCs is a cost-efficient and effective way of fine-tuning the PVs' luminous environment. To date, reports focused on non-wearable concepts; either the attached PVs were bulky and rigid,[18,19] *e.g.*, silicon-based PVs, or the material choice for the LSC polymer matrix was sturdy and solid,[20,21] like poly(methyl methacrylate). Integrated PV–LSC architectures with flexible, lightweight, and breathable abilities remained elusive. A careful selection of LSC matrix materials is paramount for maintaining the agility of textile integration in wearable electronics. In this regard, LSCs with wearable polymer matrices, such as amphiphilic polymer co-networks (APCNs), fall into the spotlight.[22–24] The biphasic APCNs are elastic, flexible, permeable to small molecules, and puncture-resistant coatings for textiles.[24,25] Furthermore, APCNs are capable of loading apolar dyes into the hydrophobic polydimethylsiloxane (PDMS) phase and allow water vapor permeability using the hydrophilic hydroxyethyl acrylate (HEA) phase, which is an essential requirement for the textile application.

In this work, fiber solar cells are integrated with flexible LSCs to realize a wearable energy harvesting textile, as shown in Fig. 1(b). A fiber dye-sensitized solar cell (FDSSC) was used as the model due to the cell stability and the excellent PCE performance.[26,27] The FDSSCs are prepared by twisting a dye absorbed photoanode fiber and a carbon nanotube fiber counter electrode as shown in Fig. 1(c). The LSCs based on APCNs have a 50 : 50 hydrophobic and hydrophilic phase volume ratio and are doped with coumarin 6 (C6), as shown in Fig. 1(d). In addition, in order to monitor the C6 luminous effect on the FDSSCs using the attached LSCs, two types of dyes with different spectral responsive characteristics, namely N719 and Y123, are selected. N719 is the most commonly used dye in dye-sensitized solar cells for its stability and mature preparation process and Y123 is selected for its relatively simple synthetic procedure. And with the combination of cobalt electrolyte high power conversion efficiency can be achieved. We selected both dyes not only due to their unique properties and prevailing usage in the DSSCs field, but also the absorbance spectrum difference, to monitor the different PCE performances under LSC attachment. The absorbance spectrum of C6, N719, and Y123 and the photoluminescence emission spectrum of C6 are shown in Fig. 1(e). Furthermore, to gain an insight into how the re-emitted light from the LSCs works on the FDSSCs, the PCE enhancement is investigated at three LSC-attachment-positions with respect to the FDSSCs (side, top, and bottom). Moreover,

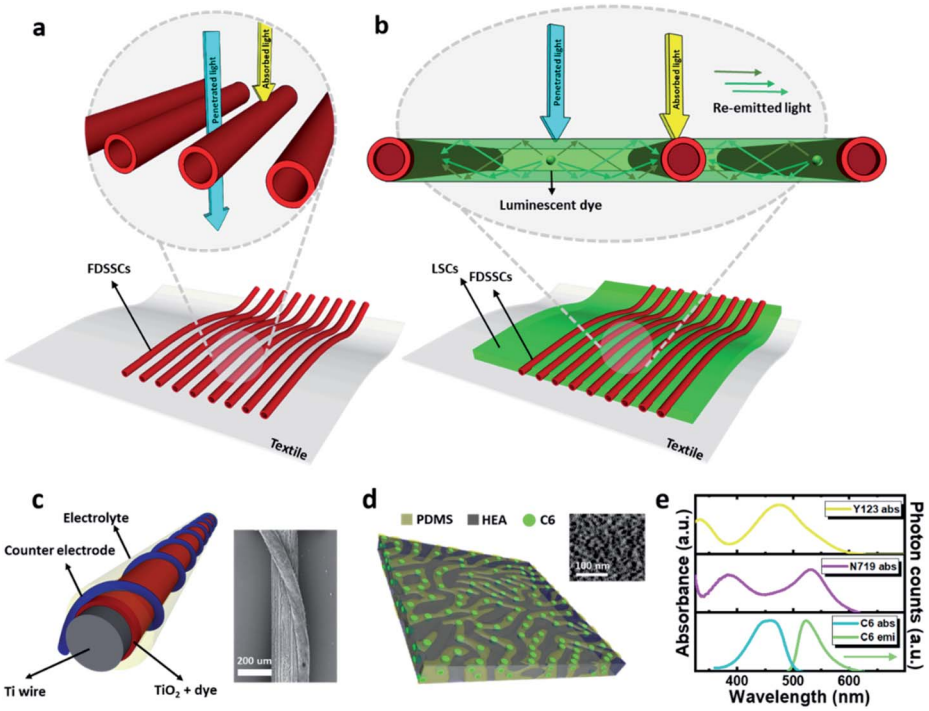

Fig. 1 Energy harvesting textile device overview, working principle, and device component details. (a) Schematic of the FDSSC array on a textile; (inset) the scheme showing the large loss of light due to gaps between fibers. (b) Schematic of LSCs integrated with FDSSCs on a textile; (inset) the utility of LSCs for collecting the penetrated light and hence the use of the whole surface area of the FDSSCs. (c) Schematic of an FDSSC and scanning electron microscope image of a modified titanium wire photoanode twisted with a carbon nanotube fiber counter electrode. (d) Schematic and atomic force microscope image of LSCs based on APCNs with nano-domains. (e) Absorbance spectrum of coumarin 6 (C6) and two types of dyes (N719 and Y123) for FDSSCs, and the photoluminescence emission spectrum of C6.

experimental data were corroborated by simulations – Monte-Carlo ray tracing has been done to visualize photons' propagation and termination within the device. This is the first experimental demonstration and computational elaboration of FDSSC and wearable LSC integration as energy harvesting textiles, fostering future progress in this arena.

Results and discussion

FDSSC–LSC attachment geometries

Reports on the integration of LSCs with planar and rigid PVs are ubiquitous in the literature.[28–31] However, the integration of wearable LSCs and thread-like FDSSCs with a curved surface area has not been reported. Here, to get a fundamental picture of the luminous effect of the LSCs on FDSSCs, three basic attachment geometries, side, top, and bottom, have been examined. The prepared LSCs were cut into several sizes and attached to N719 and Y123 based FDSSCs. For the synthesis and fabrication of the LSC film and FDSSCs, we refer the reader to the ESI (1).† All FDSSC specimens are 15 mm in length and 1 mm in diameter. The PCEs of the FDSSCs were recorded, before and after the LSC attachment, to evaluate the effect of the luminous environment changes. Moreover, to have a statistically reliable experimental value to perform further comparisons with the simulation results and to explain the mechanism, eight to eleven experiments for each sample were done. All the raw data, the used parameters, and the defining equations as well as the individual FDSSCs' EQE and dark current can be found in the ESI (2).† A Monte Carlo ray-tracing simulation has been performed for each set of empirical results to assist in explaining, visualizing and further relating the photons' propagation within the LSCs to the PCE variation of FDSSCs. Simulation details are provided in the ESI (3).† In addition, for all the measurements, the open-circuit voltage (V_{oc}) is maintained while the short circuit currents (I_{sc}) are varied under the various attachment conditions of APCN LSCs to FDSSCs. This implies that the intrinsic property of the FDSSCs is not altered by the attachment of LSCs, and thus the changes of PCE, *i.e.*, the changes of individual FDSSC power output, are solely from the variation in the luminous environment.

Side. Five lengths, 0, 0.5, 1, 1.5, and 2 cm, of LSCs were side-attached to an FDSSC and tested, as shown in Fig. 2(a). The raw data and statistical information can be found in Tables S1, S2, S7, and S8.† A higher I_{sc} in the device with LSCs than bare FDSSCs has been observed, as displayed in the current density–voltage (*J*–*V*) curve in Fig. 2(b), resulting in a higher PCE. Remarkably, the improvement for N719 and Y123 is up to 42% and 36%, respectively. The curves of the PCE enhancement *versus* various LSC lengths are logarithmic for both FDSSCs, as shown in Fig. 2(c). This is due to the nature of the luminescent materials' self-absorption within the LSC matrix, which presents exponentially decayed emission intensity with regard to the travel distance of a re-emitted photon.[19] Moreover, both N719 and Y123 FDSSCs achieved remarkable PCE enhancement, with the enhancement for the former (42%) being superior to the latter (36%). This is attributed to the absorbance range difference, *i.e.*, spectral responsiveness, of these two solar cell dyes, as shown in Fig. 1(e). The emission wavelength of C6 is nearer to the absorbance of N719 than Y123. Therefore, the re-emitted photons from C6, which reached FDSSCs from side-attached LSCs, can induce more efficient photoelectric transfer in the N719 than the Y123 solar cell dye.

Furthermore, the utilized surface areas of the FDSSCs without, with one-side, and with two-side attached LSCs have been computationally visualized from the terminated photons on the surface of FDSSCs, as depicted in Fig. 2(d). The impinging photon direction is normal to the *x*–*y* plane, *i.e.*, from the *z*-axis. Apparently, with the projected photon coordination on each plane, the side-attached LSCs not only increased the number of harvested photons, but also utilized the unused facedown part of FDSSCs, *i.e.*, the right-side-attached LSCs enable the right-facedown-side of FDSSCs to receive incoming photons. Additionally, it should be noted that, for two-side attached FDSSCs, the side-harvested photon number is doubled. Hence, PCE enhancement is rationally doubled as well, *e.g.*, the PCE enhancement for N719 and Y123 was measured to be 84% and 76%, respectively (Fig. S6†). The side-attached LSC has demonstrated a drastic PCE enhancement *via* enhancing the light-harvesting areas and re-directing the light to exploit the whole surface area of FDSSCs.

Top. The scheme of the top attached LSCs is shown in Fig. 3(a). Three different thicknesses (200, 400, and 600 μm) of LSCs were tested. The raw data and statistical information can be found in Tables S3, S4, S7, and S8.† The effect of top-covered LSCs on the FDSSCs' PCE is negative, as the current density dropped with an increase in LSC thickness, as shown in Fig. 3(b). This is attributed to the fact that not only photons from the LSCs are re-emitted, but also photons from the solar light are absorbed and terminated (*i.e.* without re-emission) in the LSCs. Fig. 3(c) shows the curves of PCE difference at various

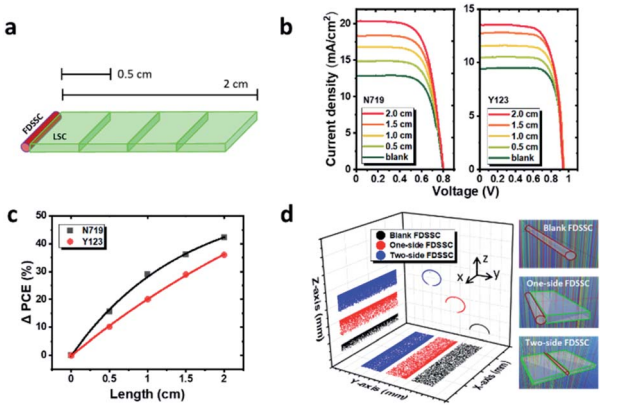

Fig. 2 The influence of side-attached LSCs on FDSSC performance. (a) Scheme of the influence of side-attached LSCs with various lengths on an FDSSC. (b) *J*–*V* curves of N719 and Y123 based FDSSCs at various lengths of attached LSCs. (c) The enhanced PCE over the length of attached LSCs with exponential decay fitted curves. (d) A ray-tracing simulation and visualization of the coordination projection of the photons that reached the FDSSC surface without, with one-side, and with two-side attached LSCs. The FDSSC with two-side LSCs attached has in-coming photons from all directions, around 360°. The photon incoming direction is the *z*-axis.

covered LSC thicknesses. The curve of N719 based FDSSCs has a relatively smoother initial PCE drop compared to Y123 based FDSSCs. This can be explained by the change of photon numbers in each wavelength, after passing through LSCs to FDSSCs.

In the range of C6 absorption (*ca.* 400–500 nm), the incoming light intensity is hence reduced. As for the C6 emission (*ca.* 500–600 nm), the light intensity increases. From the ray-tracing simulation, by extracting information from the terminated photons in the FDSSC model, the wavelength of each terminated photon can be recorded. The blocked and re-emitted photons crossing various wavelengths under the different cover thicknesses of LSCs are shown in Fig. 3(d). The number of photons at the wavelengths between 500 and 600 nm indeed rises; however, this increase does not compensate the drastic plunge between 400 and 500 nm at greater thicknesses. Besides, more photons are wave-guided to the sides of LSCs with thicker LSCs. This is another reason for the loss of light from the top-covered LSCs. Hence, a good usage of the re-emitted light wavelength (500–600 nm) of N719 leads to a smaller drop for 200 μm but still cannot compensate for all the terminated light. Consequently, from the top-covered thickness of 400 μm on, when the re-emitted light is much less prominent than the terminated light, a bigger PCE drop is expected. The top-covered results show, in principle, a negative effect on FDSSCs due to the imbalance of re-emitted and blocked photons. In the future, these issues could be tackled by placing a dichroic mirror or Bragg reflector on top of the device to harness the wave-guided lost photons, as already applied for tandem-attached LSCs for planar PVs.[17,22,32,33]

Bottom. The scheme of the bottom attached LSCs is shown in Fig. 4(a). Four different positions of APCN LSCs were tested, including one directly at the bottom (position 1) and three extended lengths (positions 2, 3 and 4) with each having a size of 15 mm length, 1 mm width, and 200 μm thickness. The raw data and statistical information can be found in Tables S5, S6, S7, and S8.† The I_{sc} increased with more attached bottom LSCs, as the current density increased as shown in Fig. 4(b). In addition, as shown in Fig. 4(c), the PCE enhancement varied with different positions. For the direct-down piece (position 1), PCE slightly increased, for the 1st extension position (position 2), a surge in PCE enhancement can be found, and for the 2nd and 3rd extensions (position 3 and 4), there is slight enhancement. Generally speaking, the increased PCE can be attributed to the photons that are not in accordance with the total internal reflection within the waveguide matrix, escaped from the top surface of APCN LSCs, and ended up being absorbed by the FDSSCs. For APCNs with a refractive index of 1.45, the escape-angle of total internal reflection is less than 45° to the normal vector. This means, theoretically, the escaped light from more than double the fiber width, *i.e.*, from the 2nd position on (>1 mm further away from the 1 mm diameter FDSSCs), should not reach the fiber and result in a PCE enhancement. However, from the experimental results, the PCE is still improved. This is attributed to the propagation of photons from greater distances to FDSSCs and the associated re-absorption/re-emission by the luminescent moieties near the FDSSCs. The photon paths are illustrated in Fig. 4(d). The photon paths indicate that the photons can either directly escape the polymer matrix or propagate internally and then escape. In both cases, photons can be eventually absorbed by the FDSSCs at a reasonable distance. The bottom results demonstrate that the lost

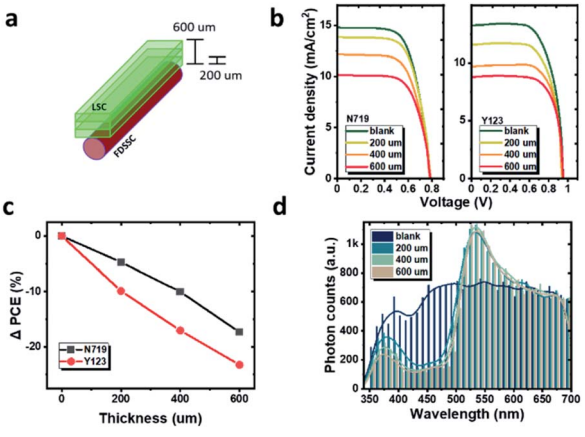

Fig. 3 The influence of the top covered LSCs on FDSSC performance. (a) Scheme of the influence of the top covered LSCs with various thicknesses on FDSSCs. (b) *J*–*V* curves of N719 and Y123 based FDSSCs with various thicknesses of top covered LSCs. (c) Reduced PCE over various thicknesses of top covered LSCs (lines to guide the eye only). (d) The counts and wavelength of photons terminated on FDSSC surfaces *via* ray-tracing simulation. The imbalanced counts of blocked (400–500 nm) and re-emitted (500–600 nm) photons of top-covered LSCs caused a negative effect on FDSSC performance.

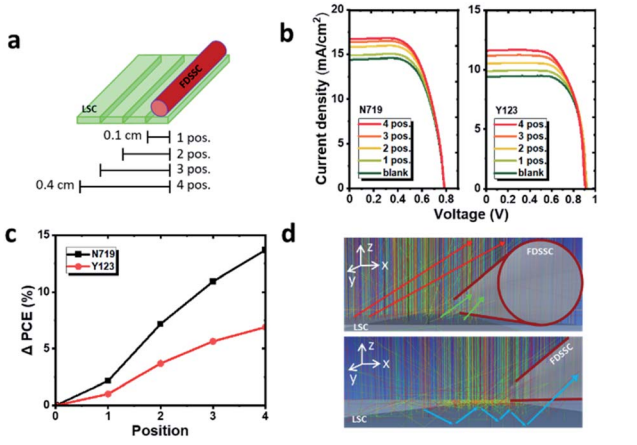

Fig. 4 The influence of bottom attached LSC position on FDSSC performance. (a) Scheme of bottom attached LSCs with various positions to FDSSCs. (b) *J*–*V* curves of N719 and Y123 based FDSSCs at various bottom positions of LSCs. (c) Enhanced PCE at various bottom positions of LSCs (lines to guide the eye only). (d) Illustration of the photon propagation paths based on ray-tracing simulation. Green arrows are the escaped light in close distance with the escaping angle and site that can be absorbed by FDSSCs, red arrows are the escaped light at a greater distance with respect to the escaping angle and site that cannot reach the FDSSCs, and the blue arrow is the propagated, re-absorbed, re-emitted light with suitable escaping angle and site and can be absorbed by the FDSSCs. The incoming photon direction is the *z*-axis.

penetrated photons can also be effectively recycled and essentially enable the photon harvesting by the face-down part of the FDSSCs.

Device performance

In the previous section, the fundamental investigation of the APCN LSC luminous effect on FDSSCs has been done experimentally and computationally with three geometries. In this section, the focus will be on the performance of the integrated device (FDSSCs with LSCs) from the perspective of device efficiency, wearability, and multiple FDSSC device optimization and power output.

Device efficiency. After the FDSSC PCE enhancement for each geometry and the ability of APCN LSCs to exploit the whole surface area of FDSSCs, the next step is to quantify the FDSSC–LSC device efficiency: concentration factor (C) and optical efficiency (η_{opt}). C gives information on the real increase in power output with respect to pristine PVs, and η_{opt} embodies the efficiency of each step that the incident photons have to go through, *i.e.*, absorption, emission, re-absorption, re-emission, and propagation within LSCs. The calculation has been carried out with the geometry of side-attached N719 based FDSSCs and a 3 cm^2 LSC size. Based on the experimental setups, the area of LSCs ($A_{LSC} = 3$ cm^2) is illuminated using a solar simulator with a power density of $I = 100$ mW cm^{-2} (AM 1.5 Global standard) and attached with FDSSCs with a diameter of 1 mm, *i.e.*, the edge area of the LSCs ($A_{FDSSCs} = 0.15$ cm^2). No further optical assistance, such as reflectors or back diffusers, is used to imitate the real working conditions of the device on textiles. Based on the photocurrent output with LSCs (I_{LSCs}) and without LSCs (I_{FDSSCs}), the concentration factor ($C = I_{LSCs}/I_{FDSSCs}$) is calculated as 1.39. Furthermore, the optical efficiency ($\eta_{opt} = C/G$) is calculated as 6.95%, where G is the geometry factor ($G = A_{LSCs}/A_{FDSSCs}$). The considerable high C and η_{opt} are principally due to the ability of the fiber structure of the FDSSCs to absorb light from all directions, allowing PVs to utilize direct incident photons and the re-emitted photons from LSCs. Furthermore, under the same illumination area, by simply shifting the FDSSC fiber to the middle of the LSCs along the x-axis, the calculated resulting efficiency is 13% higher, *i.e.*, C is 1.57 and η_{opt} is 7.85%. This category of middle placed single PVs and the consequence on efficiency enhancement are unique and limited to the fiber shaped solar cells. The device efficiency evidences a clear advantage of integrating LSCs into FDSSCs compared to conventional planar PVs. The comparison of both C and η_{opt} with values from the literature is shown in Table 1.

Device wearability. To further evaluate the device (FDSSCs with LSCs) compatibility with curved wearable surfaces like textiles, the PCE difference of the device under various bending conditions has been investigated. Fig. 5(a) shows that the PCE variation over various bending angles is less than 20% at 180° of bending. This drop can be ascribed to not only the bending angle effects on the light-absorbing projection areas, but also the increased light propagation losses within the waveguide of LSCs. Besides, as shown in Fig. 5(b), the device has maintained a PCE value of ~90% after 1000 cycles of bending at a 90° bending angle. We also investigated the water vapor permeation of the APCN LSCs in comparison with PDMS, a siloxane-based resin previously used for flexible LSCs.[34,35] The APCN matrix has a water vapor permeation 27% higher (at 35 °C) than PDMS (Fig. S3†). Moreover, by tailoring the volume ratio and/or hydrophilicity of the hydrophilic polymer phase in the APCNs, the networks' permeability can be further modified.[25,36] Besides, APCNs can be covalently bound to textiles by plasma activation of the textile surface and proceeding with the polymerization steps as shown in Fig. S2.†[24] In summary, the combination of APCN LSCs and FDSSCs provides a truly wearable solution for a device that could be directly applied along with other wearable electronics.

Multiple FDSSC device

Finally, the device with multiple FDSSCs has been demonstrated as a proof of concept of the integrated device and an example of the device optimization. Firstly, to discover the best arrangement of each fiber geometry with regard to the LSCs (Table S9†) and the fibers' packing density (Table S10†), instead of conducting copious experiments, ray-tracing simulation has been performed for efficient screening of fiber placement. The ray-tracing screening process for optimization is shown in the ESI (3).† After the screening, with five FDSSCs and one LSC of 2 × 1.5 cm^2, the configuration 4 in Table S10† of two FDSSCs placed at the side and three to the top of the LSCs shows the highest enhancement of photon harvesting ability and thus is used for an experimental build-up device. In Fig. 5(c), the voltage and power output dependence on the number of FDSSCs in series is shown. Both the device voltage and power output increase linearly, with FDSSCs in series and increasing the numbers from left to right (Table S10,† configuration 4). With increased number of FDSSCs under a certain LSC area, all the FDSSCs could simultaneously benefit from the waveguided and re-emitted light. Furthermore, the power of the device before the LSC attachment is 0.76 mW and goes up to 0.89 mW after the attachment, with a maintained voltage of 4.0 V. The 0.13 mW power output enhancement, under a small harvesting area of 3 cm^2, is a huge leap of the device's electric profile. It further enables the device to power up more wearable electronics per area, *e.g.*, a fiber memristor operates at 0.3 V and 100 pW,[37] a fiber LED requires 0.05 mW per 3 cm,[38] fiber sensors working at 1 V for various chemicals,[39,40] fiber transistors function between 0.4 and 0.6 V,[41] and the electricity can also be stored in fiber batteries.[42] This multi-FDSSC and LSC integrated device with an optimized configuration and packing density, shown in Fig. 5(d), demonstrates the potential of good integration from the perspective of wearability, power output, and scale-up ability, for future electronic wearables.

Experimental section

Fiber dye-sensitized solar cells

The fiber solar cells' photoanode fibers were composed of titanium wires modified with titanium dioxide nanotube arrays prepared *via* an anodic oxidation method. TiO_2 nanotube arrays

Table 1 Summary of the optical-electro efficiencies of FDSSCs and planar PVs with LSCs

Geometry	LSCs	Luminophores	G	C	η_{opt} (%)	Notes
FDSSCs-side	Flexible and wearable	Dye	20	1.39	6.95	This work
FDSSCs-mid			20	1.57	7.85	This work
Planar PVs-side	Rigid	Dye	6.25	0.11	1.8	*Adv. Energy Mater.*, 2015, **5**, 1500818
		QD	10	0.61	6.1	*Adv. Energy Mater.*, 2016, **6**, 1501913
			32	0.87	2.7	*Nat. Energy*, 2016, **1**, 16157
			11.5	0.33	2.85	*Nat. Photonics*, 2017, **11**, 177
			48	1.7	3.5	*Nat. Photonics*, 2018, **12**, 105
		Perovskite	12.5	0.18	1.44	*Nat. Energy*, 2019, **4**, 197.

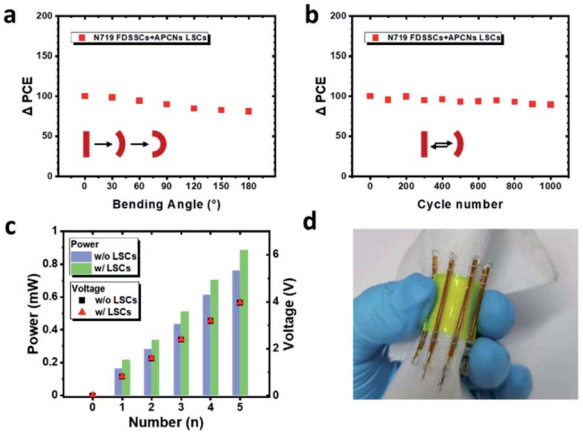

Fig. 5 Device flexibility and multiple FDSSC–LSC demonstration. PCE changes of the FDSSC–LSC device (a) at various bending angles and (b) over various bending cycles at 90° bending angle. (c) Voltage and power profile of the device with increasing number of FDSSCs on the same LSC. For identification of fiber number, we refer the reader to Table S9,† configuration 4. (d) Photograph of the FDSSC–LSC integrated device on a textile.

with diameters of approximately 100 μm acted as the electron transport layers and dye-absorber layers, and the length of TiO_2 nanotubes can be tuned by altering the anodization time. In this work, approx. 30 μm length was used. The counter electrodes were prepared from multi-walled carbon nanotube (CNT) fibers made in our previous work.[43] The CNT fiber was twined around the Ti/TiO_2 wire after soaking in a dye solution (N719 or Y123). The fiber solar cell was set into a transparent tube with an inner diameter of 600 μm and an outer diameter of 1000 μm. The I^-/I_3^- based electrolyte was matched with the N719-absorbed photoanodes, and the Co^{2+}/Co^{3+} based electrolyte was matched with the Y123-absorbed photoanodes. Images of TiO_2 nanotube structures, Fig. S1(a),† and CNT morphologies, Fig. S1(b),† can be found in the ESI (1).†

Amphiphilic polymer conetworks

The detailed APCN synthetic procedure is presented in the ESI (1)† and in our previous studies.[22,23,36,44] Herein, only the principle synthesis strategy of dye doped APCNs is described. Firstly, trimethylsilyl hydroxyethyl acrylate (TMS-HEA), methacryloxypropyl-terminated, and poly(dimethylsiloxane) (MA-PDMS-MA) were mixed and sonicated, followed by UV curing with a spacer to define the thickness. The hydrophobic TMS masking group on HEA allows miscibility with the hydrophobic PDMS during curing. After UV curing, free-standing hydrophobic networks (pre-APCNs) are formed. Later, the TMS masking group was cleaved off under acidic conditions, which leads to phase-separation due to the propelling forces triggered by the hydrophobicity difference of cross-linked poly(HEA) and PDMS, forming APCNs. After the APCNs are formed, in the last step, the hydrophobic coumarin 6 (C6) is loaded *via* swelling of the PDMS phase in toluene solution. The synthesis scheme is shown in Fig. S2.†

Conclusions

With a judicious modification of the luminous environment, the PCE of FDSSCs can be considerably enhanced, *i.e.*, up to 84%. The enhancements are attributed to the enlarged photon harvesting area, appropriate spectral responsiveness matching, and recycling of the lost photons. From the ray-tracing simulations, the digitally visualized photons show that the presence of LSCs can effectively re-emit photons to the face-down parts of FDSSCs, fully utilizing the advantage of rod-shaped FDSSCs. This renders a remarkable device concentration factor of 1.57 and optical efficiency of 7.85%, much higher than the reported planar PVs–LSCs. Furthermore, with a flexible and wearable polymer matrix, *i.e.*, APCNs, the addition of LSCs can maintain the bendability of FDSSCs. The proof-of-concept model demonstrates a power output of up to 0.89 mW at 3 cm^2 size. This is the first proposed prototype of the combination of FDSSCs and LSCs for wearable energy harvesting, from nanoscale electronic and photonic component design to light management and device integration. In this study, the integration of FDSSCs and LSCs is thoroughly investigated, to give future wearable electronics design an insightful perspective and an efficacious way of harvesting solar energy. In the future application, more work on detailed engineering could be carried out for optimizing the number of FDSSCs per LSCs and the suitable attachment geometries for specific connections with other electronic wearables, *e.g.*, fiber sensors, fiber diodes, or fiber batteries.

Author contributions

C.-S. Huang: conceptualization, methodology, validation, formal analysis, investigation, writing – original draft

preparation, writing – review & editing; X. Kang: conceptualization, methodology, validation, formal analysis, investigation, writing – original draft preparation, writing – review & editing; R. M. Rossi: supervision, writing – review & editing; M. V. Kovalenko: supervision, writing – review & editing, X. Sun: conceptualization, funding acquisition, project administration, supervision, writing – review & editing, H. Peng: project administration, funding acquisition, writing – review & editing; L. F. Boesel: conceptualization, funding acquisition, project administration, supervision, writing – review & editing.

Conflicts of interest

There are no conflicts to declare.

Notes and references

1 S. A. Hashemi, S. Ramakrishna and A. G. Aberle, *Energy Environ. Sci.*, 2020, **13**, 685–743.
2 Q. Huang, D. Wang and Z. Zheng, *Adv. Energy Mater.*, 2016, **6**, 1600783.
3 Y. Khan, A. E. Ostfeld, C. M. Lochner, A. Pierre and A. C. Arias, *Adv. Mater.*, 2016, **28**, 4373–4395.
4 B. O'regan and M. Grätzel, *Nature*, 1991, **353**, 737–740.
5 W. Song, X. Yin, D. Liu, W. Ma, M. Zhang, X. Li, P. Cheng, C. Zhang, J. Wang and Z. L. Wang, *Nano Energy*, 2019, **65**, 103997.
6 Z. Yang, J. Deng, X. Sun, H. Li and H. Peng, *Adv. Mater.*, 2014, **26**, 2643–2647.
7 X. Fu, H. Sun, S. Xie, J. Zhang, Z. Pan, M. Liao, L. Xu, Z. Li, B. Wang, X. Sun and H. Peng, *J. Mater. Chem. A*, 2018, **6**, 45–51.
8 X. Fang, Z. Yang, L. Qiu, H. Sun, S. Pan, J. Deng, Y. Luo and H. Peng, *Adv. Mater.*, 2014, **26**, 1694–1698.
9 H. Sun, Y. Zhang, J. Zhang, X. Sun and H. Peng, *Nat. Rev. Mater.*, 2017, **2**, 1–12.
10 Z. Gao, P. Liu, X. Fu, L. Xu, Y. Zuo, B. Zhang, X. Sun and H. Peng, *J. Mater. Chem. A*, 2019, **7**, 14447–14454.
11 P. Liu, Z. Gao, L. Xu, X. Shi, X. Fu, K. Li, B. Zhang, X. Sun and H. Peng, *J. Mater. Chem. A*, 2018, **6**, 19947–19953.
12 M. G. Debije, R. C. Evans and G. Griffini, *Energy Environ. Sci.*, 2021, **14**, 293–301.
13 F. Meinardi, F. Bruni and S. Brovelli, *Nat. Rev. Mater.*, 2017, **2**, 1–9.
14 I. Papakonstantinou, M. Portnoi and M. G. Debije, *Adv. Energy Mater.*, 2021, **11**, 2002883.
15 R. Mazzaro and A. Vomiero, *Adv. Energy Mater.*, 2018, **8**, 1801903.
16 B. McKenna and R. C. Evans, *Adv. Mater.*, 2017, **29**, 1606491.
17 D. R. Needell, C. R. Bukowsky, S. Darbe, H. Bauser, O. Ilic and H. A. Atwater, *IEEE Journal of Photovoltaics*, 2019, **9**, 397–401.
18 F. Meinardi, S. Ehrenberg, L. Dhamo, F. Carulli, M. Mauri, F. Bruni, R. Simonutti, U. Kortshagen and S. Brovelli, *Nat. Photonics*, 2017, **11**, 177–185.
19 K. Jakubowski, C.-S. Huang, A. Gooneie, L. F. Boesel, M. Heuberger and R. Hufenus, *Mater. Des.*, 2020, **189**, 108518.
20 M. Peng, X. Yu, X. Cai, Q. Yang, H. Hu, K. Yan, H. Wang, B. Dong, F. Zhu and D. Zou, *Nano Energy*, 2014, **10**, 117–124.
21 M. Peng, S. Hou, H. Wu, Q. Yang, X. Cai, X. Yu, K. Yan, H. Hu, F. Zhu and D. Zou, *J. Mater. Chem. A*, 2014, **2**, 926–932.
22 C.-S. Huang, K. Jakubowski, S. Ulrich, S. Yakunin, M. Clerc, C. Toncelli, R. M. Rossi, M. V. Kovalenko and L. F. Boesel, *Nano Energy*, 2020, **76**, 105039.
23 L. F. Boesel, S. Ulrich and N. Bruns, in *Amphiphilic Polymer Co-networks: Synthesis, Properties, Modelling and Applications*, ed. C. S. Patrickios, Royal Society of Chemistry, 2020, ch. 15, pp. 331–363.
24 M. Rother, J. Barmettler, A. Reichmuth, J. V. Araujo, C. Rytka, O. Glaied, U. Pieles and N. Bruns, *Adv. Mater.*, 2015, **27**, 6620–6624.
25 K. Schöller, S. Küpfer, L. Baumann, P. M. Hoyer, D. de Courten, R. M. Rossi, A. Vetushka, M. Wolf, N. Bruns and L. J. Scherer, *Adv. Funct. Mater.*, 2014, **24**, 5194–5201.
26 J. Lee, B. Llerena Zambrano, J. Woo, K. Yoon and T. Lee, *Adv. Mater.*, 2020, **32**, 1902532.
27 L. Wang, X. Fu, J. He, X. Shi, T. Chen, P. Chen, B. Wang and H. Peng, *Adv. Mater.*, 2020, **32**, 1901971.
28 H. Hernandez-Noyola, D. H. Potterveld, R. J. Holt and S. B. Darling, *Energy Environ. Sci.*, 2012, **5**, 5798–5802.
29 F. Meinardi, Q. A. Akkerman, F. Bruni, S. Park, M. Mauri, Z. Dang, L. Manna and S. Brovelli, *ACS Energy Lett.*, 2017, **2**, 2368–2377.
30 Y. Liu, N. Li, R. Sun, W. Zheng, T. Liu, H. Li, Y. Chen, G. Liu, H. Zhao and H. Liu, *Nano Energy*, 2021, 105960.
31 H. Zhao, R. Sun, Z. Wang, K. Fu, X. Hu and Y. Zhang, *Adv. Funct. Mater.*, 2019, **29**, 1902262.
32 D. R. Needell, N. Bronstein, A. P. Alivisatos, H. A. Atwater, R. Nuzzo, H. Bauser, O. Ilic, J. He and L. Xu, *IEEE Journal of Photovoltaics*, 2019, **9**, 397–401.
33 D. R. Needell, O. Ilic, C. R. Bukowsky, Z. Nett, L. Xu, J. He, H. Bauser, B. G. Lee, J. F. Geisz, R. G. Nuzzo, A. P. Alivisatos and H. A. Atwater, *IEEE Journal of Photovoltaics*, 2018, **8**, 1560–1567.
34 I. A. Carbone, K. R. Frawley and M. K. McCann, *Int. J. Photoenergy*, 2019, **2019**, 8680931.
35 M. Buffa, S. Carturan, M. Debije, A. Quaranta and G. Maggioni, *Sol. Energy Mater. Sol. Cells*, 2012, **103**, 114–118.
36 S. Ulrich, A. Sadeghpour, R. M. Rossi, N. Bruns and L. F. Boesel, *Macromolecules*, 2018, **51**, 5267–5277.
37 X. Xu, X. Zhou, T. Wang, X. Shi, Y. Liu, Y. Zuo, L. Xu, M. Wang, X. Hu and X. Yang, *Angew. Chem., Int. Ed.*, 2020, **59**, 12762–12768.
38 X. Shi, Y. Zuo, P. Zhai, J. Shen, Y. Yang, Z. Gao, M. Liao, J. Wu, J. Wang, X. Xu, Q. Tong, B. Zhang, B. Wang, X. Sun, L. Zhang, Q. Pei, D. Jin, P. Chen and H. Peng, *Nature*, 2021, **591**, 240–245.
39 L. Wang, S. Xie, Z. Wang, F. Liu, Y. Yang, C. Tang, X. Wu, P. Liu, Y. Li and H. Saiyin, *Nat. Biomed. Eng.*, 2020, **4**, 159–171.

40 L. Wang, L. Wang, Y. Zhang, J. Pan, S. Li, X. Sun, B. Zhang and H. Peng, *Adv. Funct. Mater.*, 2018, **28**, 1804456.
41 X. Wu, J. Feng, J. Deng, Z. Cui, L. Wang, S. Xie, C. Chen, C. Tang, Z. Han and H. Yu, *Sci. China: Chem.*, 2020, **63**, 1281–1288.
42 L. Li, L. Wang, T. Ye, H. Peng and Y. Zhang, *Small*, 2021, 2005015.
43 P. Liu, Y. Li, Y. Xu, L. Bao, L. Wang, J. Pan, Z. Zhang, X. Sun and H. Peng, *Small*, 2018, **14**, 1702926.
44 S. Ulrich, A. Osypova, G. Panzarasa, R. M. Rossi, N. Bruns and L. F. Boesel, *Macromol. Rapid Commun.*, 2019, 1900360.